Application of a novel haplotype-based scan for local adaptation to study high-altitude adaptation in rhesus macaques

Zachary A. Szpiech,[1,2,3,4] (iD) Taylor E. Novak,[3,*] (iD) Nick P. Bailey,[3,*] (iD) and Laurie S. Stevison[3,5] (iD)

[1]Department of Biology, Pennsylvania State University, University Park, Pennsylvania 16801

[2]Institute for Computational and Data Sciences, Pennsylvania State University, University Park, Pennsylvania 16801

[3]Department of Biological Sciences, Auburn University, Auburn, Ala 36842, USA

[4]E-mail: szpiech@psu.edu

[5]E-mail: lss0021@auburn.edu

When natural populations split and migrate to different environments, they may experience different selection pressures that can lead to local adaptation. To capture the genomic patterns of a local selective sweep, we develop XP-nSL, a genomic scan for local adaptation that compares haplotype patterns between two populations. We show that XP-nSL has power to detect ongoing and recently completed hard and soft sweeps, and we then apply this statistic to search for evidence of adaptation to high altitude in rhesus macaques. We analyze the whole genomes of 23 wild rhesus macaques captured at high altitude (mean altitude > 4000 m above sea level) to 22 wild rhesus macaques captured at low altitude (mean altitude < 500 m above sea level) and find evidence of local adaptation in the high-altitude population at or near 303 known genes and several unannotated regions. We find the strongest signal for adaptation at EGLN1, a classic target for convergent evolution in several species living in low oxygen environments. Furthermore, many of the 303 genes are involved in processes related to hypoxia, regulation of ROS, DNA damage repair, synaptic signaling, and metabolism. These results suggest that, beyond adapting via a beneficial mutation in one single gene, adaptation to high altitude in rhesus macaques is polygenic and spread across numerous important biological systems.

KEY WORDS: Adaptation, EGLN1, genome-scan, high-altitude, macaque, selection.

Impact Summary

When positive selection is ongoing or a beneficial mutation has recently fixed in a population, genetic diversity is reduced in the vicinity of the adaptive allele, and we expect to observe long homozygous haplotypes at high frequency. Here, we develop a statistic that summarizes these expected patterns and compares between two populations in order to search for evidence of adaptation that may have occurred in one but not the other. We implement this statistic in a popular and easy-to-use software package, and then apply it to study adaptation to high altitude in rhesus macaques.

*Equal Contribution

Extreme environments pose a challenge to life on multiple fronts. Very high-altitude environments are one such example, with low atmospheric oxygen, increased ultraviolet light exposure, harsh temperatures, and reduced nutrition availability. In spite of these challenges, many plants and animals, including humans, have genetically adapted to cope with these hardships. Here we study two populations of rhesus macaques, one living at high altitude and one living close to sea level. We apply our novel statistic to compare their haplotype patterns between them to search for evidence of genetic changes that are indicative of adaptation to their environment.

We find evidence for adaptation at a critical gene that helps control physiological response to low-oxygen, one that has been the target of repeated convergent evolution across

1

many species. We also find evidence for positive selection across a range of traits, including metabolic and neurological. This work helps to explain the evolutionary history of the rhesus macaque and furthers our understanding about the ways organisms genetically adapt to high-altitude environments.

Selective sweeps produce regions of reduced genetic diversity in the vicinity of an adaptive mutation. These patterns manifest as long extended regions of homozygous haplotypes segregating at high frequency (Przeworski 2002; Sabeti et al. 2002; Kim and Nielsen 2004; Garud et al. 2015). In the event of a de novo mutation that is adaptive in a population, we expect the haplotype it resides on to rapidly rise in frequency in the population (called a "hard" sweep). On the other hand, if an ancestrally segregating neutral or mildly deleterious allele turned out to be adaptive in a new environment, it would likely reside on two or more haplotypes, which would rapidly rise in frequency in the population (called a "soft" sweep) (Hermisson and Pennings 2005; Pennings and Hermisson 2006). As both of these processes happen on a time scale faster than mutation or recombination can act to break up the sweeping haplotypes, we expect to observe long and low diversity haplotypes at high frequency in the vicinity of an adaptive mutation. However, if this mutation either does not exist or is not adaptive in a sister population, we would not expect a sweep to occur and thus we would not expect to observe similar haplotype patterns.

To capture these haplotype patterns and contrast them between a pair of populations, we develop XP-nSL, a haplotype-based statistic with good power to detect partial, fixed, and recently completed hard and soft sweeps by comparing a pair of populations. XP-nSL is an extension of nSL (Ferrer-Admetlla et al. 2014) and does not require a genetic recombination map for computation. The lack of dependence on a recombination map is important, as other statistics for identifying positive selection are biased toward low-recombination regions (O'reilly et al. 2008), but the approach taken by nSL has been shown to be more robust (Ferrer-Admetlla et al. 2014). Both nSL and XP-nSL summarize haplotype diversity by computing the mean number of sites in a region that are identical-by-state across all pairs of haplotypes. Although nSL contrasts between haplotype sets carrying an ancestral or a derived allele in a single population, XP-nSL contrasts between haplotype sets in two different populations, allowing it to detect local adaptation.

An extreme example of adaptation to a local environment is the transition to high-altitude living. Organisms living at high altitudes are confronted with many challenges, including a low-oxygen atmosphere and increased ultraviolet light exposure, and these harsh environments inevitably exert strong selection pressure. Indeed, adaptation to high-altitude living has been studied

extensively across many organisms from plants, including monocots (Gonzalo-Turpin and Hazard 2009; Ahmad et al. 2016) and dicots (Kim and Donohue 2013; Liu et al. 2014; Munne-Bosch et al. 2016; Guo et al. 2018), to numerous animals including amphibians (Yang et al. 2016), canids (Li et al. 2014; Wang et al. 2014; Wang et al. 2020), humans (Bigham et al. 2009; Bigham et al. 2010; Xu et al. 2010; Yi et al. 2010; Peng et al. 2011; Huerta-Sanchez et al. 2013; Huerta-Sanchez et al. 2014; Jeong et al. 2014), yaks (Qiu et al. 2012), birds (Cai et al. 2013; Qu et al. 2013; Wang et al. 2015; Graham and Mccracken 2019), boars (Li et al. 2013), mice (Storz et al. 2007; Cheviron et al. 2012; Schweizer et al. 2019; Storz et al. 2019; Velotta et al. 2020), moles (Campbell et al. 2010), antelope (Ge et al. 2013), and horses (Hendrickson 2013). Liu et al. (2018) recently sequenced and published the whole genomes of 79 wild-born Chinese rhesus macaques collected from multiple sites in China. Among these animals, 23 were sampled from far western Sichuan province in a region with a mean altitude > 4000 m above sea level (Liu et al. 2018), providing an opportunity to study the genetics of local adaption to high altitude in rhesus macaques.

Rhesus macaques are the second most widely distributed primate, with a range extending from Afghanistan to Vietnam and from a latitude of 15 to 38 degrees north (Fooden 2000). Early ancestors of the macaque migrated out of Africa to the Eurasian continent approximately 7 million years ago—the earliest catarrhine fossils on the continent are macaque-like (Stewart and Disotell 1998). Modern rhesus macaques trace a recent origin to Southeast Asia, with a major migratory split occurring approximately 162,000 years ago separating the ancestors of modern Indian and Chinese rhesus macaques (Hernandez et al. 2007). Macaques have proven to be quite evolutionarily successful, demonstrating ecological flexibility and adaptability via developmental plasticity and behavioral changes (Richard et al. 1989; Madrid et al. 2018). Other studies have looked at how the rhesus macaque radiation has led to population-level adaptation to climate and food availability (Liu et al. 2018).

Here, we test and evaluate our XP-nSL statistic and apply it to study the genomic consequences of high-altitude living in the rhesus macaque. We use it to compare the haplotype patterns of the 23 animals from the high-altitude population with another 22 that Liu et al. (2018) sampled in lower-lying regions in eastern China with a mean altitude < 500 m above sea level.

Methods

DATA PREPARATION

Liu et al. (2018) generated whole-genome sequencing data for 79 Chinese macaques and called all biallelic polymorphic sites according to GATK best practices using rheMac8, identifying 52,534,348 passing polymorphic autosomal sites. We then
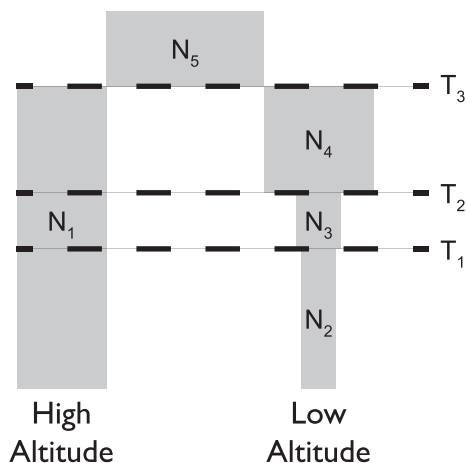
Figure 1. A representation of the demographic history for our high- and low-altitude populations as inferred by Liu et al. (2018).

Table 1. Demographic parameters used for simulations with 95% confidence intervals from (Liu et al. 2018). T values are given in number of generations before present. N values represent diploid effective population size.

Parameter	Value	95% CI
T_1	4, 660	(651, 5034)
T_2	5, 605	(3962, 10468)
T_3	9, 468	(4563, 14047)
N_1	16, 188	(8255, 26825)
N_2	3, 730	(660, 5006)
N_3	4, 506	(572, 124135)
N_4	20, 768	(1710, 88242)
N_5	66, 210	(20581, 301430)

filter all loci with >10% missing data leaving 35,639,395 biallelic sites. Next, the program SHAPEIT version 4.1.2 (Delaneau et al. 2019) was used to phase haplotypes in the full data set with a genetic map that was available for rheMac8 (Bcm-Hgsc 2020). SHAPEIT performs imputation during phasing for any missing genotypes. Our analyses here focus on 45 of the 79 samples from Liu et al. (2018), representing 23 from high-altitude regions of China (*M. m. lasiotis*) and 22 from low-altitude regions of China (*M. m. littoralis*), based on capture location information. See Table S1 for individual IDs used.

Liu et al. (2018) also inferred joint demographic histories for their five populations, and we extract the demographic parameters for our two of interest. This demographic history is recapitulated in Figure 1 with detailed parameters given in Table 1, which are then used for simulations to test XP-nSL.

A STATISTIC FOR DETECTING LOCAL ADAPTATION

We developed a cross-population haplotype-based statistic, XP-nSL, to scan for regions of the genome implicated in local adapta-

tion between two populations by extending nSL (Ferrer-Admetlla et al. 2014), each of which is defined below.

Consider the sets $A(k)$ and $D(k)$, representing the set of haplotypes at site k carrying the ancestral or derived allele, respectively, and let $n_A(k) = |A(k)|$ and $n_D(k) = |D(k)|$. Next $L_{ij}(k)$ is defined as the number of consecutive sites at which haplotype i and j are identical-by-state (IBS) in the interval containing site k. Then nSL at site k is $nS_L(k) = \log \frac{SL_A(k)}{SL_D(k)}$, where $SL_A(k) = \binom{n_A(k)}{2}^{-1} \sum_{i<j \in A(k)} L_{ij}(k)$ and $SL_D(k) = \binom{n_D(k)}{2}^{-1} \sum_{i<j \in D(k)} L_{ij}(k)$. $SL_A(k)$ and $SL_D(k)$ represent the mean $L_{ij}(k)$ over all pairs of haplotypes carrying either the ancestral or derived allele at locus k, respectively. nSL scores are then normalized genome-wide in site-frequency bins either with respect to the empirical background or neutral simulations with a matching demographic history. The nSL computation is illustrated in Ferrer-Admetlla et al. (2014). nSL is implemented in nsl (Ferrer-Admetlla et al. 2014) and selscan version 1.1.0+ (Szpiech and Hernandez 2014).

XP-nSL is defined similarly, except instead of comparing sets of haplotypes containing ancestral or derived alleles, it compares sets of haplotypes between two different populations. Let $P_1(k)$ and $P_2(k)$, represent the set of haplotypes at site k in population 1 and population 2, respectively, and let $n_{P_1}(k) = |P_1(k)|$ and $n_{P_2}(k) = |P_2(k)|$. Then XP-nSL at site k is $XPnS_L(k) = \log \frac{SL_{P_1}(k)}{SL_{P_2}(k)}$, where $SL_{P_1}(k) = \binom{n_{P_1}(k)}{2}^{-1} \sum_{i<j \in P_1(k)} L_{ij}(k)$ and $SL_{P_2}(k) = \binom{n_{P_2}(k)}{2}^{-1} \sum_{i<j \in P_2(k)} L_{ij}(k)$. $SL_{P_1}(k)$ and $SL_{P_2}(k)$ represent the mean $L_{ij}(k)$ over all pairs of haplotypes in population 1 or population 2 at locus k, respectively. XP-nSL scores are then normalized genome-wide either with respect to the empirical background or neutral simulations with a matching demographic history. The XP-nSL computation is illustrated in Fig. 2 with a toy example. We implement XP-nSL in selscan version 1.3.0+ (Szpiech and Hernandez 2014) to facilitate wide adoption. It is worth noting that XP-nSL is analogous to XP-EHH (Sabeti et al. 2007) as nSL is analogous to iHS (Voight et al. 2006).

The goal of these statistics is to capture a signal of extended regions of low diversity on sweeping haplotypes (emblematic of an ongoing or recently completed selective sweep) within a population (nSL) or on sweeping haplotypes in one population versus another (XP-nSL). When XP-nSL scores are positive this suggests evidence for a hard or soft sweep in population 1, and when XP-nSL scores are negative this suggests evidence for a hard or soft sweep in population 2.

SIMULATIONS

In order to test the ability of XP-nSL to detect ongoing and recently completed hard and soft sweeps, coalescent simulations were performed conditional on an allele frequency trajectory with
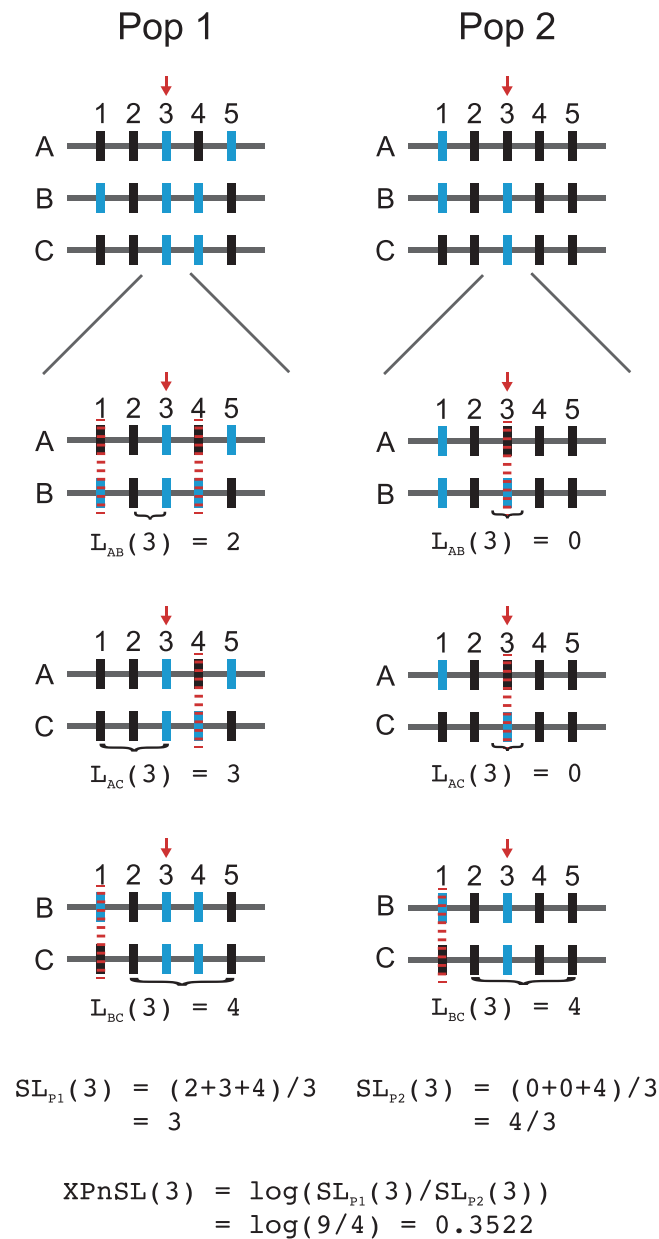
Figure 2. A toy example illustrating the computation of XP-nSL at a single site in two populations with three haplotypes (grey horizontal bars labeled A-C) and five sites (vertical bars labeled 1-5) where different alleles are colored blue or black. XP-nSL is calculated at site 3 (marked by red arrow). In each population, for each pair of haplotypes, the number of identical-by-state (IBS) sites are counted extending out from and including the test site (red arrow) until reaching a non-IBS site (marked by red dotted line). Within each population, the mean number of IBS sites is calculated across all pairs of haplotypes, and then the log-ratio of the mean from each population is computed to get XP-nSL at site 3.

the program discoal (Kern and Schrider 2016). discoal simulates an allele frequency trajectory for a single non-neutral allele backward in time and then simulates a neutral coalescent process conditional on this trajectory. This takes advantage of the speed and efficiency of the coalescent while still being able to simulate genetic diversity patterns in the vicinity of a non-neutral locus.

All simulations were run with a two-population divergence demographic history (Fig. 1 and Table 1), as inferred by Liu et al. (2018), and given by the following discoal command line arguments -p 2 46 44 -en 0 1 0.230410476572876 -en 0.071964666275442 1 0.278345739259351 -en 0.086558359329153 1 1.282885999320505 -ed 0.146214905642895 1 0 -en 0.146214905642895 0 4.089940389782871. Here, 46 haplotypes were sampled from population 0, which has the demographic history of the high-altitude population, and 44 haplotypes were sampled from population 1, which has the demographic history of the low-altitude population. A mutation rate of $\mu = 2.5 \times 10^{-8}$ (Fan et al. 2018) was used, along with a recombination rate of $r = 5.126 \times 10^{-9}$, which was computed as the genome-wide mean rate from the rheMac8 recombination map (Bcm-Hgsc 2020). A 500 kb region was simulated, thus giving a scaled mutation rate and scaled recombination parameters for discoal as -t 809.425 -r 165.967. 5,349 replicates of neutral sequence were simulated under this model, representing approximately the entire macaque genome minus 500 kb. Thus, the total simulated length of all neutral regions plus one selected region is approximately equal to the macaque genome length.

For non-neutral simulations, sweep scenarios were simulated with a positive additive selection coefficient $s \in \{0.01, 0.02, 0.05\}$, which is provided to discoal as a scaled selection coefficient $2N_1s \in \{323.77, 647.54, 1618.85\}$ (discoal flag -a). Soft sweeps are simulated as a mutation that arose neutral and turned beneficial at a particular establishment frequency $e \in \{0.01, 0.02, 0.03, 0.04, 0.05, 0.10, 0.20\}$ (discoal flag -f). Hard sweeps are simulated from a *de novo* mutation that was never neutral, that is, $e = 0$. Finally, sweeps were conditioned on having either reached a certain frequency in the population at the time of sampling, $f \in \{0.7, 0.8, 0.9, 1.0\}$ (discoal flag -c), or that the adaptive mutation reached fixation some number of generations prior to sampling, $g \in \{50, 100, 200\}$, which is provided to discoal in coalescent units $g/2N_1 \in \{1.5443 \times 10^{-3}, 3.0886 \times 10^{-3}, 6.1774 \times 10^{-3}\}$ (discoal flag -ws). For the sake of being conservative in our estimation of power (Voight et al. 2006; Sabeti et al. 2007), it was assumed the actual adaptive mutation remains unsampled (discoal flag -h), even though whole-genome sequencing data are being analyzed. For each combination of parameter values, 500 replicates were simulated.

NEUTRAL SIMULATIONS OF MISMATCHED HISTORIES

We also generate neutral simulations for three mismatched demographic histories, in order to study how a mismatched demographic history may influence the power and false positive rates of XP-nSL if used as a normalization baseline. We name these mismatched histories "Rand", "Under", and "Over" and generate 5,349 replicates for each one.

For the "Rand" history, each parameter is (uniformly) randomly chosen from within the 95% CI as inferred by (Liu et al. 2018) (see Table 1). The parameters are resampled for each replicate of the "Rand" history, and the condition $T_1 < T_2 < T_3$ is enforced. For the "Under" history, the present-day population size parameters N_1 and N_2 are the only ones modified. They are set to $N_1 = 8,255$ at the extreme low end of the 95% CI and $N_2 = 5,006$ at the extreme high end of the 95% CI. This represents a scenario where the difference in population sizes is underestimated. For the "Over" history, once again the present-day population size parameters N_1 and N_2 are the only ones modified. They are set to $N_1 = 26,825$ at the extreme high end of the 95% CI and $N_2 = 660$ at the extreme low end of the 95% CI. This represents a scenario where the difference in population sizes is overestimated.

DETECTING LOCAL ADAPTATION IN REAL DATA

From the phased data set, animals captured at high altitude (n = 23) and animals captured at low altitude (n = 22) were subset (see Table S1). Using selscan version 1.3.0 (Szpiech and Hernandez 2014) to compute raw XP-nSL scores across the genome (selscan flags –xpnsl –vcf high-altitude.vcf –vcf-ref low-altitude.vcf), scores were then normalized using the genome-wide empirical background with selscan's norm version 1.3.0 program (norm flag –xpnsl). The low-altitude population was used as the reference population, so positive XP-nSL scores correspond to long homozygous haplotypes and a possible sweep in the high-altitude population compared to the low-altitude population, and vice versa for negative XP-nSL scores. A Manhattan plot of genome-wide normalized XP-nSL scores > 2 is plotted in Fig. S7.

In order to identify regions implicated as potentially adaptive, we search for clusters of extreme scores along a chromosome. Using selscan's companion program norm version 1.3.0, the genome is divided into non-overlapping 100 kb regions and both the maximum XP-nSL score and the fraction of XP-nSL scores > 2 are computed (norm flags –xpnsl –bp-win –winsize 100,000). norm then creates 10 quantile bins (–qbins 10) for windows with more than 10 sites per window (–min-snps 10) and identifies the top 1% of windows with the highest fraction of extreme scores (Fig. S6 and Table S4). Each window is then annotated with the ensembl rheMac8 gene list, and a maximum XP-nSL score is assigned to a given gene based on the max-score

in the 100 kb window with which it overlaps. If a gene overlaps more than one 100 kb window, it is assigned the top max-score from among the windows.

Results

POWER ANALYSIS OF XP-NSL

First, we evaluate the performance of XP-nSL based on simulations. After computing XP-nSL for all sites in all simulations, scores were normalized by subtracting the mean and dividing by standard deviation of the neutral simulations, giving the neutral scores an approximately N(0,1) distribution (Fig. S1).

We consider the maximum score in a 100 kb interval as a way to identify regions under positive selection similar to Voight et al. (2006). To get the null distribution of max-scores, the maximum score is computed in the central 100 kb of each neutral simulation. The distribution of max-scores in neutral simulations had a median of 2.093 with 95% of the mass between 0.804 and 3.492, which is represented in Figure 3 as a solid horizontal black line (median) and two dashed horizontal black lines (95% interval). Next, the maximum score is computed in the central 100 kb of all non-neutral simulations, and the median and 95% intervals are plotted for each parameter combination. Figure 3 shows good separation between the neutral distribution of max-scores and the distribution of max-scores for a range of non-neutral parameters, suggesting that our statistic can distinguish between neutral and non-neutral scenarios. Note that soft sweeps that start at 0.1 or 0.2 frequency see the least separation from the neutral distribution. To evaluate the power of the max-score statistic, the 99th percentile of the max-score distribution is computed in the neutral distribution ($neutral_{99} = 3.792$) and power is calculated as the mass of each non-neutral max score distribution $> neutral_{99}$. With this approach, even if the entire genome is neutrally evolving, at most 1% of the genome will be identified as putatively under selection thus fixing the false positive rate at 1% at most. Results are plotted in Figure 4A, which shows good power to detect both incomplete and completed sweeps. For soft sweeps that start at a frequency ≤ 0.03, power is $> 75\%$ when the sweep is near or just past fixation; the ability to detect soft sweeps falls off for sweeps that start > 0.03 frequency.

Next, we consider that due to linkage disequilibrium consecutive scores will be correlated, and we should therefore expect clusters of extreme scores in true non-neutral regions. We thus consider a window-based approach to identify selected regions similar to Voight et al. (2006), where the top 1% windows with a high number of extreme scores are identified. Taking the central 100 kb region of each simulation, the fraction of XP-nSL scores > 2 (representing approximately the highest 2% of all neutral scores) is computed. Since each 100 kb window has a
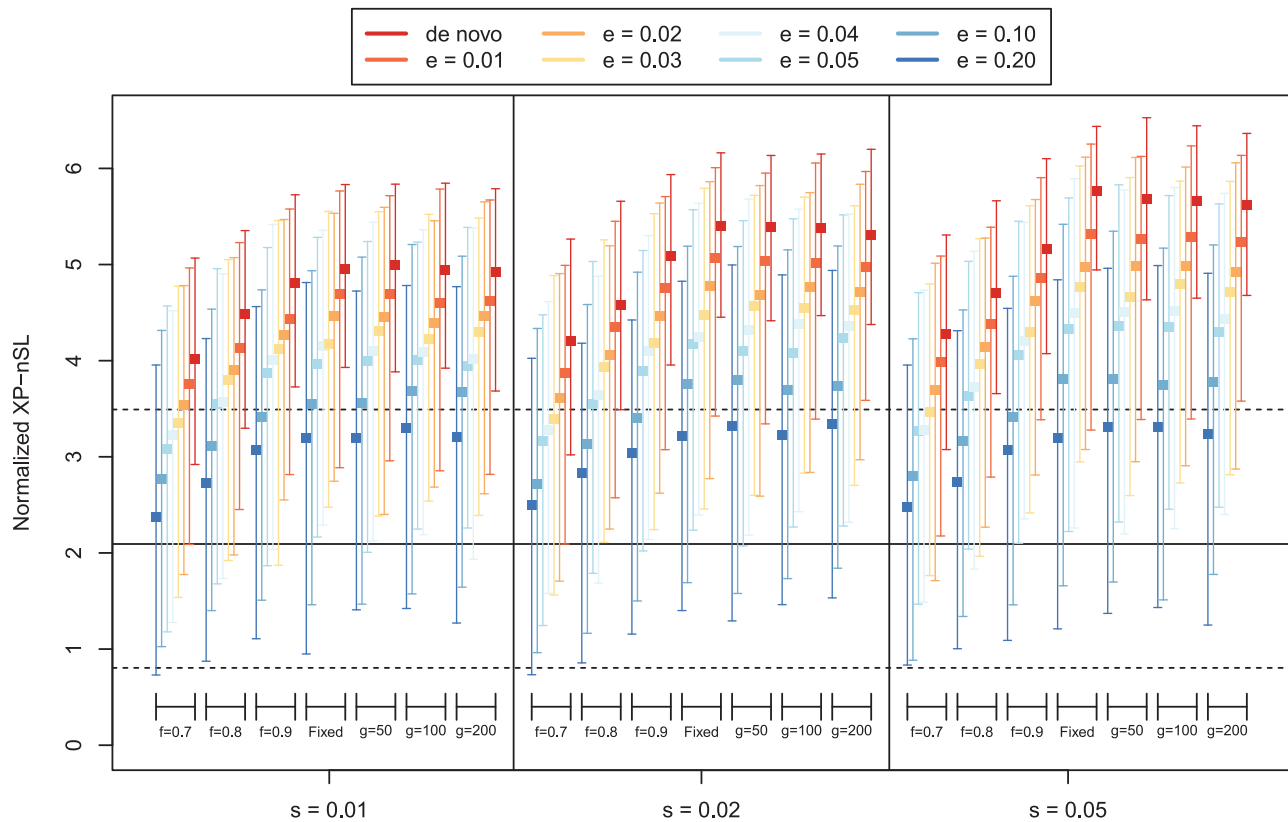
Figure 3. The distribution of maximum XP-nSL scores from simulations across various parameters, represented by medians and intervals containing 95% of the mass of the distribution. Neutral simulations are represented by the black solid horizonal line (median) and the black dashed horizonal line (95% interval). Non-neutral simulations represented by a colored box (median) and error bars (95% interval). The parameters are e (frequency at which selection begins, e > 0 indicates soft sweep), f (frequency of selected mutation at sampling), g (number of generations since fixation), and s (selection coefficient).

variable number of sites within it, windows with fewer sites are more likely to have a higher fraction of extreme scores by chance. Thus, windows are binned by a number of sites into 10 quantile bins, and the top 1% of windows with the highest fraction of extreme scores in each bin establishes the threshold beyond which a window is taken as putatively selected, as in Voight et al. (2006). With this approach, even if the entire genome is neutrally evolving, at most 1% of the genome will be identified as putatively under selection thus fixing the false positive rate at 1% at most. Power is computed for each non-neutral parameter set as the proportion of replicates for which the central 100 kb exceeds the 1% threshold as calculated from neutral simulations. The results are plotted in Figure 4B, which shows improved power over the max-score approach across a wider range of parameters. Indeed, using the window-based method, power to detect soft sweeps improves substantially across the parameter space, with > 75% power to detect soft sweeps at or near fixation that started at frequency ≤ 0.05.

We next consider how XP-nSL power compares to nSL, XP-EHH, and F_{ST}. We compare to nSL since XP-nSL is an exten-

sion of it, to XP-EHH as it is a similar haplotype-based two-population selection statistic, and to F_{ST} as it a popular two-population method used to infer local adaptation. For all simulations, nSL and XP-EHH are computed using selscan version 1.3.0 (Szpiech and Hernandez 2014). Normalization, identification of top windows, and power calculation were done as described above for XP-nSL. F_{ST} is computed using VCFtools version 0.1.16 (Danecek et al. 2011), which implements Weir and Cockerham's formulation (Weir and Cockerham 1984), in 100 kb windows for all simulations. The 99th percentile F_{ST} value was determined from the central 100 kb window among all neutral simulations. Power was then computed for each non-neutral parameter set as the proportion of replicates for which the F_{ST} value of the central 100 kb window is greater than the neutral threshold as calculated from neutral simulations.

Figure 5 shows the difference in power between XP-nSL and each statistic (raw power for nSL, XP-EHH, and F_{ST} shown in Fig. S4) over the simulated parameter space, where positive values indicate that XP-nSL has more power than the comparison statistic. XP-nSL is compared to nSL in Figure 5A, which
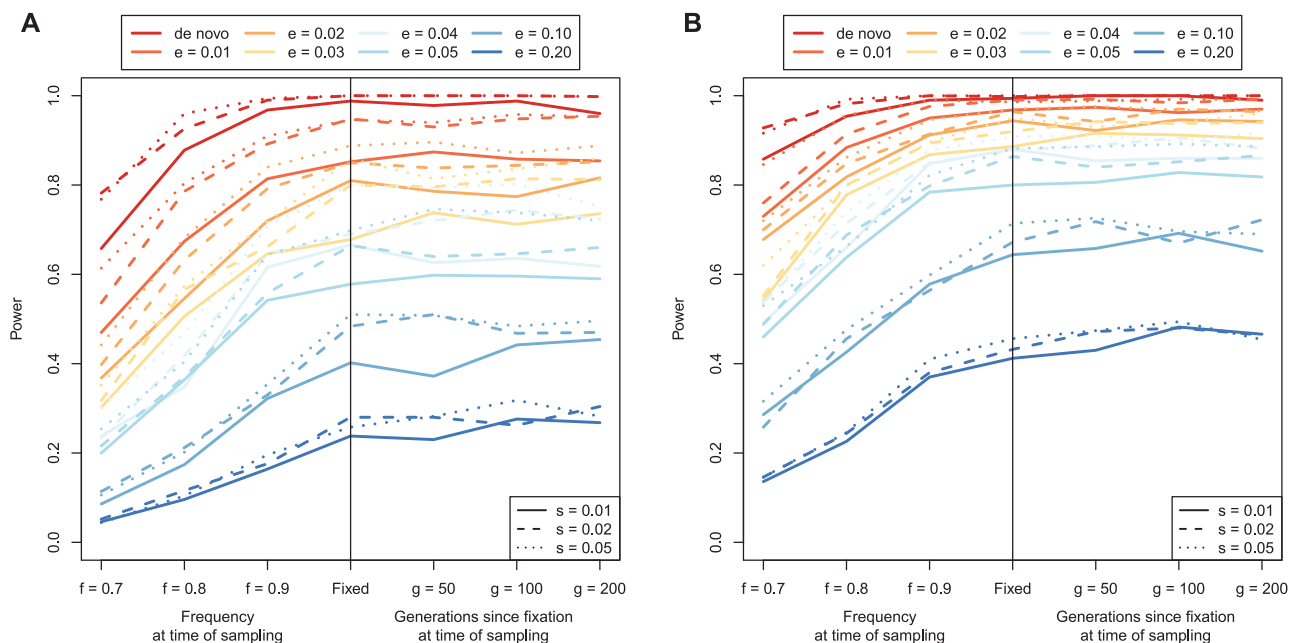
Figure 4. Power curves for (A) the max-score approach and (B) the window-based approach to identifying sweeps. The parameters are e (frequency at which selection begins, e > 0 indicates soft sweep), f (frequency of selected mutation at sampling), g (number of generations since fixation), and s (selection coefficient).

shows XP-nSL improves on nSL across nearly the entire parameter space and especially for sweeps that have fixed in the recent past. XP-nSL is compared to XP-EHH in Fig. 5B, which shows XP-nSL improving on XP-EHH for soft sweeps ($e > 0$). Finally, XP-nSL is compared to F_{ST} in Fig. 5C, which shows XP-nSL improving on F_{ST} mostly for incomplete sweeps, although F_{ST} performed better post-fixation for certain soft sweep scenarios ($e \geq 0.05$).

CAVEATS FOR USING NEUTRAL SIMULATIONS TO NORMALIZE REAL DATA

In principle, one could use matched neutral simulations as a normalization baseline when analyzing real data. However, we can only recommend this approach when the populations being studied have very well characterized (1) joint demographic histories, (2) mutation rates, and (3) recombination rates, as a mismatch can skew the power and false positive rates of the statistic. Although it is possible to fit complex demographic histories to sampled data, these inferred histories may ultimately be misspecified due to missing parameters in the underlying model or subtle violations of the standard assumptions that go into demographic history inference (Ewing and Jensen 2016; Schrider et al. 2016; Platt and Harris 2020). To illustrate how misspecification of effective population size and population split times may influence the distribution of simulated neutral XP-nSL scores, we generated three mismatched sets of neutral simulations "Rand," "Under," and "Over" (see Methods) to use as a

normalization baseline for our original simulations. Although we do not address misspecification of mutation or recombination rate here, we do note that these two processes would influence marker density and haplotype lengths under neutrality, which could ultimately have an effect on the simulated neutral XP-nSL scores.

When neutral simulations are normalized with the correct demographic history, they approximately follow a standard normal distribution (Fig. S1 and Fig. S2), however, the distribution of neutral scores gets badly distorted when one of the mismatched histories is used (Fig. S2). These distortions have practical consequences for making inferences. Power was calculated for XP-nSL using the window-based method described above but using each mismatched history as a normalization baseline (Fig. S3). The false positive rate for each scenario was also estimated by calculating the proportion of neutral simulations that are identified as under selection for each scenario (Table S2). Fig. S3A-B shows that for the "Rand" and "Under" normalization scenarios, power was greatly reduced across the whole parameter space. Only hard sweeps with the strongest selection coefficients post-fixation were likely to be identified. False positive rates for these scenarios were at 0 (Table S3), whereas for a matched history it was estimated at 9.908×10^{-3}. Fig. S3C shows that, for the "Over" normalization scenario, power was uniformly excellent, however when analyzing neutral simulations, the false positive rate was estimated at 0.9538. This suggests that using such a badly matched demographic history for normalization creates
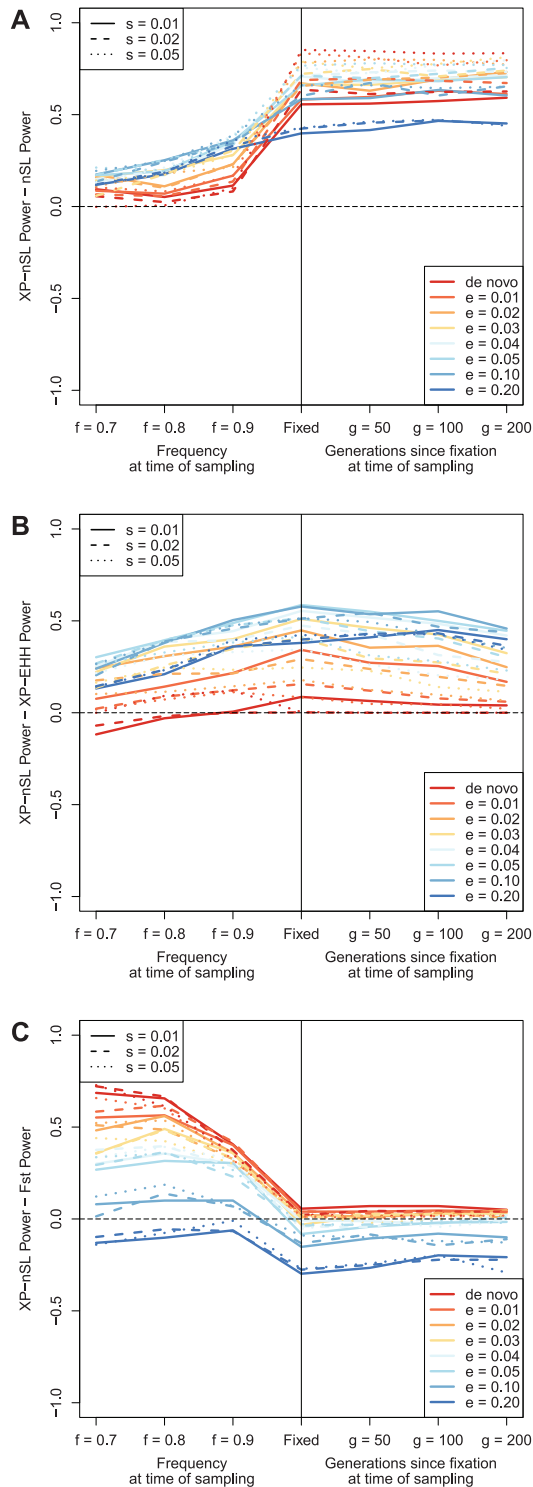
Figure 5. Difference in power between XP-nSL and (A) nSL, (B) XP-EHH, and (C) F_{ST}. Values above 0 indicate XP-nSL has more power, and values below 0 indicate XP-nSL has less power. The horizontal black dotted line marks 0. The parameters are e (frequency at which selection begins, e > 0 indicates soft sweep), f (frequency of selected mutation at sampling), g (number of generations since fixation), and s (selection coefficient).

a near complete inability to distinguish between neutral and selected regions.

IDENTIFYING EVIDENCE FOR ADAPTATION TO HIGH ALTITUDE IN RHESUS MACAQUES

Next, we analyzed the pair of rhesus macaque populations using XP-nSL, searching for evidence of local adaptation in the high-altitude population. Using the low-altitude population as the reference population, normalized $XPnS_L > 0$ corresponds to longer and higher frequency haplotypes in the high-altitude population, with very large positive scores and clusters of large scores suggesting evidence for positive selection. Dividing the genome into 100 kb windows, the maximum XP-nSL score of that region is assigned to each gene in it (see Methods), thus multiple genes may have the same max-score by virtue of being in the same 100 kb window. Genes overlapping multiple 100 kb windows were assigned the top max-score among the windows.

Using the per-gene max-scores, PANTHER (Mi et al. 2019) gene ontology categories were tested for enrichment of high scores, where significance suggests an enrichment of signals of positive selection among genes involved. Significant terms related to regulation of ion transport and synaptic signaling (Table 2), each of which are affected by hypoxic conditions (Karle et al. 2004; Corcoran and O'connor 2013).

From the genomic regions that were identified to contain a high proportion of extreme positive scores (see Methods), 303 annotated genes were found across 270 regions. A permutation test (10,000 replicates) that randomly shuffles 270 100 kb regions around the genome indicates that this is substantially fewer than one would expect by chance ($p = 1.4 \times 10^{-3}$; Fig. S5), indicating that the method is not simply randomly picking gene regions. These regions, their characteristics, and the genes contained therein are given in Table S2. A PANTHER (Mi et al. 2019) gene ontology overrepresentation test indicates a 9.04-fold enrichment of genes associated with monooxygenase activity ($FDR = 4.47 \times 10^{-2}$).

The monooxygenases in the selected regions include FMO2, FMO5, CYP2C8, CYP2C9, CYP2C93, and ENSMMUT00000011129. These genes are important for the metabolism of oxygen and the generation of reactive oxygen species (ROS) (Krueger and Williams 2005). Under the physiological stress of a low-oxygen environment, ROS levels increase and cause oxidative damage, and, in humans, long-term adaptation to high altitudes includes adaptation to oxidative damage (Janocha et al. 2017). Indeed, AOX1 is also identified in our top regions, mutations in which have been shown to affect ROS levels in humans (Foti et al. 2017).

The genome-wide top ten 100 kb windows based on the percentage of extreme XP-nSL scores are summarized in Table 3, and these windows overlap several genes, including EGLN1. The

Table 2. Gene ontology enrichment analysis results based on maximum XP-nSL scores per gene. Significant GO terms are enriched for high XP-nSL scores.

PANTHER GO-Slim Biological Process	Gene Ontology ID	p-Value	FDR
Anterograde trans-synaptic signaling	GO:0098916	4.43×10^{-5}	1.52×10^{-2}
Chemical synaptic transmission	GO:0007268	4.43×10^{-5}	1.83×10^{-2}
Regulation of transport	GO:0051049	3.60×10^{-5}	1.85×10^{-2}
Trans-synaptic signaling	GO:0099537	6.32×10^{-5}	1.86×10^{-2}
Synaptic signaling	GO:0099536	1.03×10^{-4}	2.66×10^{-2}
Ion transport	GO:0006811	1.33×10^{-4}	2.75×10^{-2}
Transmembrane transport	GO:0055085	1.57×10^{-4}	2.94×10^{-2}
Regulation of ion transport	GO:0043269	1.30×10^{-4}	2.97×10^{-2}
Metal ion transport	GO:0030001	2.21×10^{-4}	3.04×10^{-2}
Regulation of localization	GO:0032879	2.13×10^{-4}	3.14×10^{-2}
Regulation of ion transmembrane transport	GO:0034765	2.66×10^{-4}	3.23×10^{-2}
Inorganic ion transmembrane transport	GO:0098660	3.01×10^{-4}	3.45×10^{-2}
Sodium ion transport	GO:0006814	3.36×10^{-4}	3.65×10^{-2}
Ion transmembrane transport	GO:0034220	4.50×10^{-4}	4.42×10^{-2}
Regulation of transmembrane transport	GO:0034762	4.40×10^{-4}	4.54×10^{-2}
Cation transport	GO:0006812	4.87×10^{-4}	4.57×10^{-2}
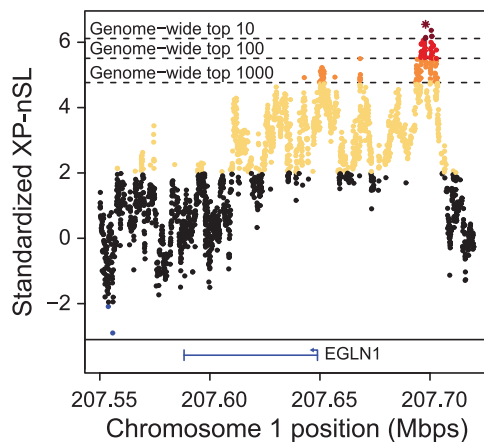
Figure 6. XP-nSL scores in the vicinity of the EGLN1 locus. This locus contains the genome wide top score (star) and six of the top ten genome wide scores (dark red).

EGLN1 locus is directly adjacent to the single strongest selection signal identified in the entire genome (Fig. 6). This region has the third-highest cluster of extreme scores (Table 3), contains the highest XP-nSL score in the entire genome (chr1:207,698,003, $XPnS_L = 6.54809$), and contains six of the top 10 genome wide XP-nSL scores (colored dark red in Fig. 6). EGLN1 is a regulator of oxygen homeostasis (To and Huang 2005) and is a classic target for adaptation to low-oxygen levels, having repeatedly been the target of adaptation in numerous organisms living at high altitude around the world (Bigham et al. 2009; Bigham et al. 2010; Jeong et al. 2014; Graham and Mccracken 2019). In addition to EGLN1, other genes related to lung function, oxygen use, and angiogenesis had evidence for local adaptation between

low- and high-altitude populations: TRPM7, RBPJ, and ENS-MMUT00000040566 (Table S2). TRPM7 downregulation in a hypoxia-induced rat model was associated with pulmonary hypertension (PAH) (Xing et al. 2019). ENSMMUT00000040566 is a MAPK6 ortholog, which interacts with EGLN3 (Rodriguez et al. 2016), and both it and RBPJ are involved in angiogenesis (Ramasamy et al. 2014).

Due to the reduced oxygen levels at high altitudes, we expect genes involved in metabolism and respiration may be under positive selection. Indeed, MDH1 encodes a critical enzyme in the citrate cycle (Tanaka et al. 1996) and is found in the top ten genome-wide regions (Table 3). A paralog of MDH1, MDH1B, has been previously identified as a target of selection in humans living at high altitude (Yi et al. 2010). ACADM and COX15 are also found in putatively adaptive regions (Table S2). Mutations in and differing expression levels of ACADM are related to oxidative stress and mitochondrial dysfunction in human disease (Xu et al. 2018). COX15 is involved in oxidative phosphorylation (Alston et al. 2017), and cytochrome c oxidase (COX) genes have previously been identified as under selection in primates relative to other mammals (Osada and Akashi 2012).

High-altitude environments present a particular metabolic challenge to organisms that must maintain a stable internal body temperature (Rosenmann and Morrison 1974; Hayes and Chappell 1986; Chappell and Hammond 2004), a result of increased oxygen demand from aerobic thermogenesis conflicting with lower oxygen availability. It has been shown that highland deer mice have adapted by increased capacity to metabolize lipids compared to lowland deer mice (Cheviron et al. 2012), and previous studies in rhesus macaques have shown there may be

Table 3. The top ten 100 kb genomic regions as ranked by percentage of scores greater than 2. Concatenated region represents the genomic region merged with adjacent top 1% regions. Max score represents the max XP-nSL score in the concatenated region. Genes gives all genes overlapping the concatenated region.

Genomic Region	% > 2	Flanking Regions	Concatenated Region	Max Score	Genes
* chr2:42300001-42400000	81.62%	3	chr2:42200001-42600000	5.42043	STXBP5L
chr3:99100001-99200000	78.18%	3	chr3:99100001-99500000	5.54282	-
chr1:207600001-207700000	***77.39%***	***1***	***chr1:207600001-207800000***	***6.54809***[†]	***EGLN1, TSNAX***
chr10:69700001-69800000	76.60%	4	chr10:69700001-70200000	4.89388	PITPNB, ENSMMUT00000079195.1, TTC28
chr13:64300001-64400000	74.01%	1	chr13:64300001-64500000	4.17728	WDPCP, MDH1, ENSMMUT00000070474.1
chr7:96400001-96500000	73.86%	1	chr7:96400001-96600000	4.58886	FAM177A1, PPP2R3C, ENSMMUT00000039911.2, ENSMMUT00000027928.3
chr10:70400001-70500000	70.24%	0	chr10:70400001-70500000	3.69192	TTC28
* chr2:42400001-42500000	65.86%	3	chr2:42200001-42600000	5.42043	STXBP5L
chr7:120400001-120500000	62.54%	0	chr7:120400001-120500000	5.86114	KIAA0586, ENSMMUT00000059161.1
chr18:20600001-20700000	62.42%	0	chr18:20600001-20700000	5.37386	RNF138

* These regions are contained in the same concatenated region.
† Top genome-wide score. This region contains 6 of the top 10 genome-wide scores.

drastic differences in diets between high-and low-altitude populations (Zhao et al. 2018). Indeed, in the high-altitude macaque population studied here, genes related to lipid and fat metabolism (DOCK7, ST6GALNAC5, ANGPTL3, and ACACA) were found in putative adaptive regions. Across human populations, these genes are all responsible for varying blood levels of fatty acids (Guo et al. 2016; Dewey et al. 2017; Hebbar et al. 2018). Furthermore, ACACA has been shown to vary fatty acid blood concentrations and be differentially expressed in highland versus lowland swine populations (Shang et al. 2019).

STXBP5L also appears in the top ten regions (Table 3) and is involved in vesicular trafficking and neurotransmitter release (Kumar et al. 2015). As primate brains use large amounts of oxygen and energy to function (Osada and Akashi 2012) signatures of selection on neurological genes may be expected across populations living at altitudes with differing oxygen levels. In addition to STXBP5L, several genes related to neural development and synaptic formation (JAG2, TRPM7, DOCK7, NSG2, AUTS2) were identified (Table S2). JAG2 is involved in the Notch signaling pathway. While Notch signaling is involved in many developmental and homeostatic processes, its role in neuronal differentiation in the mammalian brain is notable in this context (Cardenas et al. 2018). TRPM7, in addition to its association with PAH, plays a role in hypoxic neuronal cell death (Aarts et al. 2003).

DNA damage, including double-strand breaks and pyrimidine dimerization, can manifest as a result of oxidative stress (Ye et al. 2016) or increased exposure to UV radiation (Zhang et al. 2000; Greinert et al. 2012), both of which increase at high altitudes. Three DNA damage repair genes are in our set of genes identified in positively selected regions. The ring finger protein RNF138 is in our list of top 10 genomic windows (Table 3) and has been shown to promote DNA double-strand break repair (Ismail et al. 2015). Furthermore, the DNA polymerase POLH also appears in a putatively adaptive region (Table S2) and is known to be able to efficiently bypass pyrimidine dimer lesions (Zhang et al. 2000). Finally, PAXIP1 appears in Table S2 as well and has been shown to promote repair of double-strand breaks through homologous recombination (Wang et al. 2010).

Interestingly, within the putatively selected region that includes PAXIP1 is an uncharacterized long non-coding RNA (lncRNA), ENSMMUT00000081951, that was recently annotated in the rheMac10 genome build. This lncRNA has high sequence similarity to a lncRNA on the same synteny block in humans called PAXIP1-AS1. In human pulmonary artery smooth muscle cells, knockdown of PAXIP1-AS1 leads to an abnormal response to PAH where migration and proliferation of cells are reduced, and overexpression of PAXIP-AS1 leads to apoptosis resistance (Jandl et al. 2019). Although, we note that any link between PAH and ENSMMUT00000081951 in rhesus macaques is highly speculative at this point.

Discussion

When populations split and migrate, they may adapt in different ways in response to their local environments. Genetic adaptations that arise and sweep through the population leave a characteristic genomic pattern of long haplotypes of low diversity and high frequency. We develop a two-population haplotype-based statistic, XP-nSL, to capture these patterns. With good power to detect hard and soft sweeps that occur in one population but not another, XP-nSL can identify positively selected regions of the genome likely the result of local adaptation. We apply this statistic to genomes sampled from a pair of wild-born populations of Chinese rhesus macaques, inferred to have diverged approximately 9,500 generations ago, one of which lives at high altitude in far western Sichuan province, and the other that lives close to sea level.

Life at high altitude presents extreme biological challenges, including low atmospheric oxygen, increased UV exposure, harsh winters, and reduced nutrition availability, which create strong selection pressure. Organisms that survive and persist are likely to be carrying genetic mutations that confer an advantage for living in such harsh environments. Common targets for adaptation to such an environment include genes related to hypoxia, regulation of ROS, DNA damage repair, and metabolism (Cheviron and Brumfield 2012; Witt and Huerta-Sanchez 2019; Storz and Cheviron 2021). Indeed, in the high-altitude macaque population, we identify a strong signal of positive selection at the EGLN1 locus (Fig. 6), a classic target for adaptation to low-oxygen environments, in addition to 302 other genes, many of which are related to the myriad environmental selection pressures expected in high-altitude environments. As has been suggested previously for other organisms (Cheviron and Brumfield 2012; Bigham and Lee 2014; Simonson 2015; Witt and Huerta-Sanchez 2019; Storz and Cheviron 2021), these results suggest that, rather than a single adaptive mutation at a single locus, adaptation to this extreme environment by rhesus macaques is polygenic and acts through multiple biological systems.

AUTHOR CONTRIBUTIONS
Z.A.S. and L.S.S. conceived of the study. Z.A.S. performed all simulations and genomic analyses and implemented novel statistics. Z.A.S., T.E.N., and N.P.B. characterized gene functions and ontologies with contributions from L.S.S. Z.A.S. wrote the manuscript with contributions from N.P.B., T.E.N., and L.S.S. All authors read and approved the manuscript.

LITERATURE CITED

Aarts, M., K. Iihara, W. L. Wei, Z. G. Xiong, M. Arundine, W. Cerwinski, et al. 2003. A key role for TRPM7 channels in anoxic neuronal death. Cell 115:863–877.

Ahmad, K. S., M. Hameed, S. Fatima, M. Ashraf, F. Ahmad, M. Naseer, et al. 2016. Morpho-anatomical and physiological adaptations to high altitude in some Aveneae grasses from Neelum Valley, Western Himalayan Kashmir. Acta Physiol. Plant. 38:93. Available at https://link.springer.com/content/pdf/10.1007/s11738-016-2114-x.pdf

Alston, C. L., M. C. Rocha, N. Z. Lax, D. M. Turnbull, and R. W. Taylor. 2017. The genetics and pathology of mitochondrial disease. J. Pathol. 241:236–250.

BCM-HGSC. 2020. Baylor College of Medicine Human Genome Sequencing Center Rhemac8 Recombination Map. Available at: [http://ftp.hgsc.bcm.edu/ucscHub/rhesusSNVs/rheMac8/all.rate.bw].

Bigham, A., M. Bauchet, D. Pinto, X. Mao, J. M. Akey, R. Mei, et al. 2010. Identifying signatures of natural selection in Tibetan and Andean populations using dense genome scan data. PLoS Genet. 6:e1001116. Available at https://journals.plos.org/plosgenetics/article?id=10.1371/journal.pgen.1001116

Bigham, A. W., and F. S. Lee. 2014. Human high-altitude adaptation: forward genetics meets the HIF pathway. Genes Dev. 28:2189–2204.

Bigham, A. W., X. Mao, R. Mei, T. Brutsaert, M. J. Wilson, C. G. Julian, et al. 2009. Identifying positive selection candidate loci for high-altitude adaptation in Andean populations. Hum. Genomics 4:79–90.

Cai, Q., X. Qian, Y. Lang, Y. Luo, J. Xu, S. Pan, et al. 2013. Genome sequence of ground tit Pseudopodoces humilis and its adaptation to high altitude. Genome Biol. 14:R29. Available at https://genomebiology.biomedcentral.com/articles/10.1186/gb-2013-14-3-r29#citeas

Campbell, K. L., J. F. Storz, A. V. Signore, H. Moriyama, K. C. Catania, A. P. Payson, et al. 2010. Molecular basis of a novel adaptation to hypoxic-hypercapnia in a strictly fossorial mole. BMC Evol. Biol. 10:214. Available at https://bmcecolevol.biomedcentral.com/articles/10.1186/1471-2148-10-214

Cardenas, A., A. Villalba, C. de Juan Romero, E. Pico, C. Kyrousi, A. C. Tzika, et al. 2018. Evolution of Cortical Neurogenesis in Amniotes Controlled by Robo Signaling Levels. Cell 174:590–606 e521.

Chappell, M. A., and K. A. Hammond. 2004. Maximal aerobic performance of deer mice in combined cold and exercise challenges. J. Comp. Physiol. B 174:41–48.

Cheviron, Z. A., G. C. Bachman, A. D. Connaty, G. B. McClelland, and J. F. Storz. 2012. Regulatory changes contribute to the adaptive enhancement of thermogenic capacity in high-altitude deer mice. Proc. Natl. Acad. Sci. 109:8635–8640.

Cheviron, Z. A., and R. T. Brumfield. 2012. Genomic insights into adaptation to high-altitude environments. Heredity 108:354–361.

Corcoran, A., and J. J. O'Connor. 2013. Hypoxia-inducible factor signalling mechanisms in the central nervous system. Acta Physiol. 208:298–310.

Danecek, P., A. Auton, G. Abecasis, C. A. Albers, E. Banks, M. A. De-Pristo, et al. 2011. The variant call format and VCFtools. Bioinformatics 27:2156–2158.

Delaneau, O., J. F. Zagury, M. R. Robinson, J. L. Marchini, and E. T. Dermitzakis. 2019. Accurate, scalable and integrative haplotype estimation. Nat. Commun. 10:5436. Available at https://www.nature.com/articles/s41467-019-13225-y

Dewey, F. E., V. Gusarova, R. L. Dunbar, C. O'Dushlaine, C. Schurmann, O. Gottesman, et al. 2017. Genetic and Pharmacologic Inactivation of ANGPTL3 and Cardiovascular Disease. N. Engl. J. Med. 377:211–221.

Ewing, G. B., and J. D. Jensen. 2016. The consequences of not accounting for background selection in demographic inference. Mol. Ecol. 25:135–141.

Fan, Z., A. Zhou, N. Osada, J. Yu, J. Jiang, P. Li, et al. 2018. Ancient hybridization and admixture in macaques (genus Macaca) inferred from whole genome sequences. Mol. Phylogenet. Evol. 127:376–386.

Ferrer-Admetlla, A., M. Liang, T. Korneliussen, and R. Nielsen. 2014. On detecting incomplete soft or hard selective sweeps using haplotype structure. Mol. Biol. Evol. 31:1275–1291.

Fooden, J. 2000. Systematic review of the rhesus macaque, Macaca mulatta (Zimmermann, 1780). Field Museum of Natural History, Chicago, Ill.

Foti, A., F. Dorendorf, and S. Leimkuhler. 2017. A single nucleotide polymorphism causes enhanced radical oxygen species production by human aldehyde oxidase. PLoS One 12:e0182061. Available at https://journals.plos.org/plosone/article?id=10.1371/journal.pone.0182061

Garud, N. R., P. W. Messer, E. O. Buzbas, and D. A. Petrov. 2015. Recent selective sweeps in North American Drosophila melanogaster show signatures of soft sweeps. PLoS Genet. 11:e1005004. Available at https://journals.plos.org/plosgenetics/article?id=10.1371/journal.pgen.1005004

Ge, R. - L., Q. Cai, Y. - Y. Shen, A. San, L. Ma, Y. Zhang, et al. 2013. Draft genome sequence of the Tibetan antelope. Nat. Commun. 4:1858. Available at https://www.nature.com/articles/ncomms2860

Gonzalo-Turpin, H., and L. Hazard. 2009. Local adaptation occurs along altitudinal gradient despite the existence of gene flow in the alpine plant species Festuca eskia. J. Ecol. 97:742–751.

Graham, A. M., and K. G. McCracken. 2019. Convergent evolution on the hypoxia-inducible factor (HIF) pathway genes EGLN1 and EPAS1 in high-altitude ducks. Heredity 122:819–832.

Greinert, R., B. Volkmer, S. Henning, E. W. Breitbart, K. O. Greulich, M. C. Cardoso, et al. 2012. UVA-induced DNA double-strand breaks result from the repair of clustered oxidative DNA damages. Nucleic Acids Res. 40:10263–10273.

Guo, T., R. X. Yin, F. Huang, L. M. Yao, W. X. Lin, and S. L. Pan. 2016. Association between the DOCK7, PCSK9 and GALNT2 Gene Polymorphisms and Serum Lipid levels. Sci. Rep. 6:19079. Available at https://www.nature.com/articles/srep19079

Guo, X., Q. Hu, G. Hao, X. Wang, D. Zhang, T. Ma, et al. 2018. The genomes of two Eutrema species provide insight into plant adaptation to high altitudes. DNA Res. 25:307–315.

Hayes, J. P., and M. A. Chappell. 1986. Effects of Cold Acclimation on Maximum Oxygen Consumption during Cold Exposure and Treadmill Exercise in Deer Mice, Peromyscus maniculatus. Physiol. Zool. 59:473–481.

Hebbar, P., R. Nizam, M. Melhem, F. Alkayal, N. Elkum, S. E. John, et al. 2018. Genome-wide association study identifies novel recessive genetic variants for high TGs in an Arab population. J. Lipid Res. 59:1951–1966.

Hendrickson, S. L. 2013. A genome wide study of genetic adaptation to high altitude in feral Andean Horses of the paramo. BMC Evol. Biol. 13:273. Available at https://bmcecolevol.biomedcentral.com/articles/10.1186/1471-2148-13-273

Hermisson, J., and P. S. Pennings. 2005. Soft sweeps: molecular population genetics of adaptation from standing genetic variation. Genetics 169:2335–2352.

Hernandez, R. D., M. J. Hubisz, D. A. Wheeler, D. G. Smith, B. Ferguson, J. Rogers, et al. 2007. Demographic histories and patterns of linkage disequilibrium in Chinese and Indian rhesus macaques. Science 316:240–243.

Huerta-Sanchez, E., M. Degiorgio, L. Pagani, A. Tarekegn, R. Ekong, T. Antao, et al. 2013. Genetic signatures reveal high-altitude adaptation in a set of ethiopian populations. Mol. Biol. Evol. 30:1877–1888.

Huerta-Sanchez, E., X. Jin, B., Z. Asan, B. M. Peter, N. Vinckenbosch, et al. 2014. Altitude adaptation in Tibetans caused by introgression of Denisovan-like DNA. Nature 512:194–197.

Ismail, I. H., J. P. Gagne, M. M. Genois, H. Strickfaden, D. McDonald, Z. Xu, et al. 2015. The RNF138 E3 ligase displaces Ku to promote DNA end resection and regulate DNA repair pathway choice. Nat. Cell Biol. 17:1446–1457.

Jandl, K., H. Thekkekara Puthenparampil, L. M. Marsh, J. Hoffmann, J. Wilhelm, C. Veith, et al. 2019. Long non-coding RNAs influence the transcriptome in pulmonary arterial hypertension: the role of PAXIP1-AS1. J. Pathol. 247:357–370.

Janocha, A. J., S. A. A. Comhair, B. Basnyat, M. Neupane, A. Gebremedhin, A. Khan, et al. 2017. Antioxidant defense and oxidative damage vary widely among high-altitude residents. Am. J. Hum. Biol. 29.

Jeong, C., G. Alkorta-Aranburu, B. Basnyat, M. Neupane, D. B. Witonsky, J. K. Pritchard, et al. 2014. Admixture facilitates genetic adaptations to high altitude in Tibet. Nat. Commun. 5:3281. Available at https://www.nature.com/articles/ncomms4281

Karle, C., T. Gehrig, R. Wodopia, S. Hoschele, V. A. Kreye, H. A. Katus, et al. 2004. Hypoxia-induced inhibition of whole cell membrane currents and ion transport of A549 cells. Am. J. Physiol. Lung Cell. Mol. Physiol. 286:L1154–L1160.

Kern, A. D., and D. R. Schrider. 2016. Discoal: flexible coalescent simulations with selection. Bioinformatics 32:3839–3841.

Kim, E., and K. Donohue. 2013. Local adaptation and plasticity of Erysimum capitatum to altitude: its implications for responses to climate change. J. Ecol. 101:796–805.

Kim, Y., and R. Nielsen. 2004. Linkage Disequilibrium as a Signature of Selective Sweeps. Genetics 167:1513–1524.

Krueger, S. K., and D. E. Williams. 2005. Mammalian flavin-containing monooxygenases: structure/function, genetic polymorphisms and role in drug metabolism. Pharmacol. Ther. 106:357–387.

Kumar, R., M. A. Corbett, N. J. Smith, L. A. Jolly, C. Tan, D. J. Keating, et al. 2015. Homozygous mutation of STXBP5L explains an autosomal recessive infantile-onset neurodegenerative disorder. Hum. Mol. Genet. 24:2000–2010.

Li, M., S. Tian, L. Jin, G. Zhou, Y. Li, Y. Zhang, et al. 2013. Genomic analyses identify distinct patterns of selection in domesticated pigs and Tibetan wild boars. Nat. Genet. 45:1431–1438.

Li, Y., D. D. Wu, A. R. Boyko, G. D. Wang, S. F. Wu, D. M. Irwin, et al. 2014. Population variation revealed high-altitude adaptation of Tibetan mastiffs. Mol. Biol. Evol. 31:1200–1205.

Liu, J. - Q., Y. - W. Duan, G. Hao, X. - J. Ge, and H. Sun. 2014. Evolutionary history and underlying adaptation of alpine plants on the Qinghai–Tibet Plateau. J. Syst. Evol. 52:241–249.

Liu, Z., X. Tan, P. Orozco-terWengel, X. Zhou, L. Zhang, S. Tian, et al. 2018. Population genomics of wild Chinese rhesus macaques reveals a dynamic demographic history and local adaptation, with implications for biomedical research. Gigascience 7.

Madrid, J. E., T. M. Mandalaywala, S. P. Coyne, J. Ahloy-Dallaire, J. P. Garner, C. S. Barr, et al. 2018. Adaptive developmental plasticity in rhe-

sus macaques: the serotonin transporter gene interacts with maternal care to affect juvenile social behaviour. Proc. R. Soc. B 285:20180541. Available at https://royalsocietypublishing.org/doi/10.1098/rspb.2018.0541

Mi, H., A. Muruganujan, D. Ebert, X. Huang, and P. D. Thomas. 2019. PANTHER version 14: more genomes, a new PANTHER GO-slim and improvements in enrichment analysis tools. Nucleic Acids Res. 47:D419–D426.

Munne-Bosch, S., A. Cotado, M. Morales, E. Fleta-Soriano, J. Villellas, and M. B. Garcia. 2016. Adaptation of the Long-Lived Monocarpic Perennial Saxifraga longifolia to High Altitude. Plant Physiol. 172:765–775.

O'Reilly, P. F., E. Birney, and D. J. Balding. 2008. Confounding between recombination and selection, and the Ped/Pop method for detecting selection. Genome Res. 18:1304–1313.

Osada, N., and H. Akashi. 2012. Mitochondrial-nuclear interactions and accelerated compensatory evolution: evidence from the primate cytochrome C oxidase complex. Mol. Biol. Evol. 29:337–346.

Peng, Y., Z. Yang, H. Zhang, C. Cui, X. Qi, X. Luo, et al. 2011. Genetic variations in Tibetan populations and high-altitude adaptation at the Himalayas. Mol. Biol. Evol. 28:1075–1081.

Pennings, P. S., and J. Hermisson. 2006. Soft sweeps II–molecular population genetics of adaptation from recurrent mutation or migration. Mol. Biol. Evol. 23:1076–1084.

Platt, A., and D. N. Harris. 2020. Phantom histories of misspecified pasts. bioRxiv : 2020.2006.2026.173963.

Przeworski, M. 2002. The Signature of Positive Selection at Randomly Chosen Loci. Genetics 160:1179–1189.

Qiu, Q., G. Zhang, T. Ma, W. Qian, J. Wang, Z. Ye, et al. 2012. The yak genome and adaptation to life at high altitude. Nat. Genet. 44:946–949.

Qu, Y., H. Zhao, N. Han, G. Zhou, G. Song, B. Gao, et al. 2013. Ground tit genome reveals avian adaptation to living at high altitudes in the Tibetan plateau. Nat. Commun. 4:2071. Available at https://www.nature.com/articles/ncomms3071

Ramasamy, S. K., A. P. Kusumbe, L. Wang, and R. H. Adams. 2014. Endothelial Notch activity promotes angiogenesis and osteogenesis in bone. Nature 507:376–380.

Richard, A. F., S. J. Goldstein, and R. E. Dewar. 1989. Weed macaques: the evolutionary implications of macaque feeding ecology. Int. J. Primatol. 10:569. Available at https://link.springer.com/article/10.1007/BF02739365

Rodriguez, J., R. Pilkington, A. Garcia Munoz, L. K. Nguyen, N. Rauch, S. Kennedy, et al. 2016. Substrate-Trapped Interactors of PHD3 and FIH Cluster in Distinct Signaling Pathways. Cell Rep. 14:2745–2760.

Rosenmann, M., and P. Morrison. 1974. Maximum oxygen consumption and heat loss facilitation in small homeotherms by He-O2. Am. J. Physiol. 226:490–495.

Sabeti, P. C., D. E. Reich, J. M. Higgins, H. Z. Levine, D. J. Richter, S. F. Schaffner, et al. 2002. Detecting recent positive selection in the human genome from haplotype structure. Nature 419:832–837.

Sabeti, P. C., P. Varilly, B. Fry, J. Lohmueller, E. Hostetter, C. Cotsapas, et al. 2007. Genome-wide detection and characterization of positive selection in human populations. Nature 449:913–918.

Schrider, D. R., A. G. Shanku, and A. D. Kern. 2016. Effects of Linked Selective Sweeps on Demographic Inference and Model Selection. Genetics 204:1207–1223.

Schweizer, R. M., J. P. Velotta, C. M. Ivy, M. R. Jones, S. M. Muir, G. S. Bradburd, et al. 2019. Physiological and genomic evidence that selection on the transcription factor Epas1 has altered cardiovascular function in high-altitude deer mice. PLoS Genet. 15:e1008420.

Available at https://journals.plos.org/plosgenetics/article?id=10.1371/journal.pgen.1008420

Shang, P., W. Li, G. Liu, J. Zhang, M. Li, L. Wu, et al. 2019. Identification of lncRNAs and Genes Responsible for Fatness and Fatty Acid Composition Traits between the Tibetan and Yorkshire Pigs. Int. J. Genomics 2019:5070975. Available at https://www.hindawi.com/journals/ijg/2019/5070975/

Simonson, T. S. 2015. Altitude Adaptation: a Glimpse Through Various Lenses. High Alt. Med. Biol. 16:125–137.

Stewart, C. B., and T. R. Disotell. 1998. Primate evolution - in and out of Africa. Curr. Biol. 8:R582–R588.

Storz, J. F., and Z. A. Cheviron. 2021. Physiological Genomics of Adaptation to High-Altitude Hypoxia. Annu. Rev. Anim. Biosci. 9:149–171.

Storz, J. F., Z. A. Cheviron, G. B. McClelland, and G. R. Scott. 2019. Evolution of physiological performance capacities and environmental adaptation: insights from high-elevation deer mice (Peromyscus maniculatus). J. Mammal. 100:910–922.

Storz, J. F., S. J. Sabatino, F. G. Hoffmann, E. J. Gering, H. Moriyama, N. Ferrand, et al. 2007. The molecular basis of high-altitude adaptation in deer mice. PLoS Genet. 3:e45. Available at https://journals.plos.org/plosgenetics/article?id=10.1371/journal.pgen.0030045

Szpiech, Z. A., and R. D. Hernandez. 2014. selscan: an efficient multithreaded program to perform EHH-based scans for positive selection. Mol. Biol. Evol. 31:2824–2827.

Tanaka, T., J. Inazawa, and Y. Nakamura. 1996. Molecular cloning and mapping of a human cDNA for cytosolic malate dehydrogenase (MDH1). Genomics 32:128–130.

To, K. K., and L. E. Huang. 2005. Suppression of hypoxia-inducible factor 1alpha (HIF-1alpha) transcriptional activity by the HIF prolyl hydroxylase EGLN1. J. Biol. Chem. 280:38102–38107.

Velotta, J. P., C. E. Robertson, R. M. Schweizer, G. B. McClelland, and Z. A. Cheviron. 2020. Adaptive shifts in gene regulation underlie a developmental delay in thermogenesis in high-altitude deer mice. Mol. Biol. Evol, 37:2309–2321.

Voight, B. F., S. Kudaravalli, X. Wen, and J. K. Pritchard. 2006. A map of recent positive selection in the human genome. PLoS Biol. 4:e72. Available at https://journals.plos.org/plosbiology/article?id=10.1371/journal.pbio.0040072

Wang, G. D., R. X. Fan, W. Zhai, F. Liu, L. Wang, L. Zhong, et al. 2014. Genetic convergence in the adaptation of dogs and humans to the high-altitude environment of the tibetan plateau. Genome Biol. Evol. 6:2122–2128.

Wang, M. - S., Y. Li, M. - S. Peng, L. Zhong, Z. - J. Wang, Q. - Y. Li, et al. 2015. Genomic Analyses Reveal Potential Independent Adaptation to High Altitude in Tibetan Chickens. Mol. Biol. Evol. 32:1880–1889.

Wang, M. - S., S. Wang, Y. Li, Y. Jhala, M. Thakur, N. O. Otecko, et al. 2020. Ancient hybridization with an unknown population facilitated high altitude adaptation of canids. Mol. Biol. Evol..

Wang, X., K. Takenaka, and S. Takeda. 2010. PTIP promotes DNA double-strand break repair through homologous recombination. Genes Cells 15:243–254.

Weir, B. S., and C. C. Cockerham. 1984. Estimating F-Statistics for the Analysis of Population Structure. Evolution. 38:1358–1370.

Witt, K. E., and E. Huerta-Sanchez. 2019. Convergent evolution in human and domesticate adaptation to high-altitude environments. Phil. Trans. R. Soc. B 374:20180235. Available at https://royalsocietypublishing.org/doi/10.1098/rstb.2018.0235

Xing, J., M. Wang, J. Hong, Y. Gao, Y. Liu, H. Gu, et al. 2019. TRPM7 channel inhibition exacerbates pulmonary arterial hypertension through MEK/ERK pathway. Aging 11:4050–4065.

Xu, S., S. Li, Y. Yang, J. Tan, H. Lou, W. Jin, et al. 2010. A Genome-Wide Search for Signals of High-Altitude Adaptation in Tibetans. Mol. Biol. Evol. 28:1003–1011.

Xu, Z., X. Jin, W. Cai, M. Zhou, P. Shao, Z. Yang, et al. 2018. Proteomics Analysis Reveals Abnormal Electron Transport and Excessive Oxidative Stress Cause Mitochondrial Dysfunction in Placental Tissues of Early-Onset Preeclampsia. Proteomics Clin. Appl. 12:e1700165. Available at https://onlinelibrary.wiley.com/doi/full/10.1002/prca.201700165

Yang, X., Y. Wang, Y. Zhang, W. H. Lee, and Y. Zhang. 2016. Rich diversity and potency of skin antioxidant peptides revealed a novel molecular basis for high-altitude adaptation of amphibians. Sci. Rep. 6:19866. Available at https://www.nature.com/articles/srep19866

Ye, B., N. Hou, L. Xiao, Y. Xu, H. Xu, and F. Li. 2016. Dynamic monitoring of oxidative DNA double-strand break and repair in cardiomyocytes. Cardiovasc. Pathol. 25:93–100.

Yi, X., Y. Liang, E. Huerta-Sanchez, X. Jin, Z. X. Cuo, J. E. Pool, et al. 2010. Sequencing of 50 human exomes reveals adaptation to high altitude. Science 329:75–78.

Zhang, Y., F. Yuan, X. Wu, O. Rechkoblit, J. S. Taylor, N. E. Geacintov, et al. 2000. Error-prone lesion bypass by human DNA polymerase eta. Nucleic Acids Res. 28:4717–4724.

Zhao, J., Y. Yao, D. Li, H. Xu, J. Wu, A. Wen, et al. 2018. Characterization of the Gut Microbiota in Six Geographical Populations of Chinese Rhesus Macaques (Macaca mulatta), Implying an Adaptation to High-Altitude Environment. Microb Ecol. 76:565–577.

Supporting Information

Additional supporting information may be found online in the Supporting Information section at the end of the article.

Table S1. Population classification by individual ID.

Table S2. List of genomic windows with the top 1% highest fraction of extreme XP-nSL scores.

Table S3. Estimates of false positive rates for various demographic history normalization scenarios.

Table S4. Bin boundaries (# of sites), number of windows per bin, and top 1% thresholds for the XP-nSL analysis of rhesus macaques.

Figure S1. A normal quantile-quantile plot of neutral XP-nSL scores showing generally good adherence to a standard normal distribution. Due to autocorrelation along the genome, only every 1000th score is plotted.

Figure S2. The distribution of neutral XP-nSL scores normalized with a matched demographic history (solid line), normalized with the "Rand" demographic history (dashed line), normalized with the "Under" demographic history (dotted line), and normalized with the "Over" demographic history (dash-dot line). Normalizing with the wrong demographic history can dramatically shift the distribution of neutral XP-nSL scores.

Figure S3. XP-nSL power using mismatched demographic histories for normalization. (A) Using the "Rand" history. (B) Using the "Under" history. (C) Using the "Over" history.

Figure S4. Power curves for (A) nSL, (B) XP-EHH, and (C) F_{ST}. The parameters are e (frequency at which selection begins, e > 0 indicates soft sweep), f (frequency of selected mutation at sampling), g (number of generations since fixation), and s (selection coefficient).

Figure S5. A permutation test (10,000 replicates) that shuffles 270 100kb regions around the macaque genome and counts the number of unique genes overlapping. The red vertical line marks the 303 genes found in the real data analysis. The probability of observing 303 or fewer genes is 1.4×10^{-3}, indicating the analysis is not randomly choosing gene regions.

Figure S6. Proportion of scores > 2 versus number of sites in window. Blue vertical dashed lines indicate bin boundaries. Each circle is a window, red dots indicate a proportion of scores > 2 beyond the 1% threshold for that bin.

Figure S7. A Manhattan plot of normalized XP-nSL scores across the genome. Due to a very large number of points, only scores > 2 were plotted.